Valence shell electronically excited states of 1-phenylimidazole and 1-benzylimidazole

I. Powis, D. A. Shaw, D. Townsend & D. M. P. Holland

View supplementary material

Published online: 17 Jun 2024.

Submit your article to this journal

View related articles

View Crossmark data

Taylor & Francis
Taylor & Francis Group

RESEARCH ARTICLE

🔓 OPEN ACCESS | Check for updates

Valence shell electronically excited states of 1-phenylimidazole and 1-benzylimidazole

I. Powis[a], D. A. Shaw[b], D. Townsend[c,d] and D. M. P. Holland[b]

[a]School of Chemistry, The University of Nottingham, Nottingham, UK; [b]STFC, Daresbury Laboratory, Daresbury, UK; [c]Institute of Photonics and Quantum Sciences, Heriot-Watt University, Edinburgh, UK; [d]Institute of Chemical Sciences, Heriot-Watt University, Edinburgh, UK

ABSTRACT

The valence shell electronically excited states of 1-phenylimidazole and 1-benzylimidazole have been studied by employing synchrotron radiation to measure the absolute photoabsorption cross-section of each molecule, from threshold up to an energy of 10.8 eV. Assignments have been proposed for some of the broad absorption bands using calculated transition energies and oscillator strengths. Natural transition orbital plots have allowed the Rydberg and/or valence character of the electronically excited states to be assessed. Some of the calculated transitions in 1-benzylimidazole and 1-phenylimidazole have initial and final orbitals that are analogous to those of transitions in the isolated constituent rings of imidazole and benzene. Other mixed Rydberg/valence transitions, especially those leading to some of the low energy electronically excited states in 1-phenylimidazole, have an initial orbital located on the imidazole ring while valence character in the final orbital is localised on the phenyl ring. Thus, photoexcitation results in charge transfer from the donor site (imidazole) to the acceptor (the phenyl ring) in the nascent ion core of the Rydberg state. In both 1-benzylimidazole and 1-phenylimidazole the lowest energy excited state arises from a transition analogous to the $1e_{1g} \rightarrow 1e_{2u}$ $1B_{2u}$ electric dipole-forbidden transition in benzene.
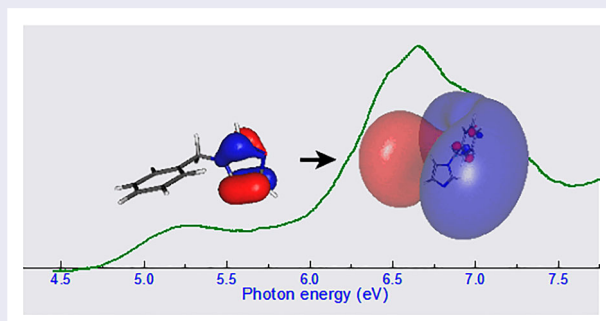
1. Introduction

In a recent investigation [1], the valence shell electronically excited states of imidazole ($C_3H_4N_2$, Scheme 1) were studied by measuring the absolute photoabsorption cross-section, and calculated transition energies and oscillator strengths were used to assign the observed structure. The broad bands appearing in the absorption spectrum were attributed to transitions into excited valence states and the superimposed sharp structure was associated with Rydberg states. An interesting aspect of that work concerned the use of Natural Transition Orbitals (NTOs) [2] to help confirm the character of the

excited state associated with a calculated transition. This proved particularly useful in assigning electronic excited states having a mixed Rydberg/valence character.

The same experimental and theoretical methods have now been employed to study the valence shell electronically excited states of 1-benzylimidazole ($C_{10}H_{10}N_2$, Scheme 1) and 1-phenylimidazole ($C_9H_8N_2$, Scheme 1). Henceforth, 1-benzylimidazole and 1-phenylimidazole will be referred to as bz-imid and ph-imid, respectively. One of the aims of the present work on bz-imid and ph-imid is to investigate the effect of the close proximity of the two ring structures (benzene/phenyl and imidazole)
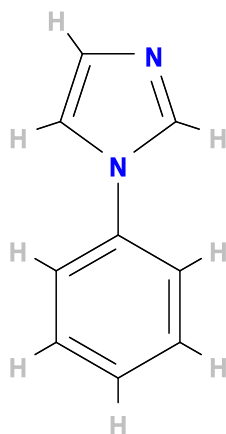
1-phenylimidazole

imidazole

1-benzylimidazole

Scheme 1. Structures of title molecules and imidazole showing atom numbering.

on the electronic transitions. For example, do some of the transitions in bz-imid or ph-imid have initial and final orbitals that resemble those of an analogous transition in benzene or imidazole? Are the excitation energies of such transitions, where the initial and final orbitals are located on the same ring, shifted to higher or lower energy compared to the excitation energy of the analogous transition in the corresponding isolated molecule? Alternatively, do some of the transitions in bz-imid or ph-mid involve initial and/or final orbitals that are delocalised over the two constituents, that cannot therefore be considered as simply associated to one of the isolated molecule components? Our NTO plots, by providing a simple visualisation of relevant orbitals, allow the nature of the transition to be characterised. Thus, the locations of the initial and final orbitals involved in a specific transition can be determined.

As our results demonstrate, especially those for ph-imid, a particularly interesting class of transition involves an initial orbital located principally on the imidazole ring, and a final orbital located primarily on the phenyl ring. Thus, photoexcitation leads to charge transfer between the two rings. Such intramolecular charge transfer processes, which may occur in molecules sufficiently large to contain two independent charge sites, are important in many biological systems and in photosynthesis [3].

The valence shell photoabsorption spectra of bz-imid and ph-imid, recorded in our study using synchrotron radiation, exhibit several bands which resemble those in the absorption spectra of benzene [4–7] (and references therein) or imidazole [1]. An understanding of the valence and Rydberg states in these two molecules is therefore a prerequisite for an interpretation of the absorption bands, and the associated excited states, in the spectra of bz-imid and ph-imid. The low energy valence excited states of benzene have been studied extensively theoretically [8–12], and indeed have been used to perform benchmark calculations of vertical excitation energies and oscillator strengths using a variety of computational methods. However, theoretical predictions for transitions into Rydberg states associated with series converging onto the $\tilde{X}$ $^2E_{1g}$ ionic state are very limited. Therefore, the present theoretical studies were extended to include the low energy valence and Rydberg states in benzene. This effort proved worthwhile because it allowed a detailed comparison to be made with the Rydberg state excitation energies [13,14] determined with resonantly-enhanced multi-photon-ionisation (REMPI) techniques. For the valence and Rydberg states of imidazole, we rely upon the experimental and theoretical results reported by Holland *et al.* [1], and an earlier examination of its ionisation energies [15].

Several computational approaches have been employed to calculate vertical transition energies and properties for the electronically excited states in bz-imid and ph-imid, aiming to achieve a balanced representation of valence and Rydberg states. This information, including oscillator strengths, is used to determine possible assignments for the observed absorption bands. Simple visualisations of the principal NTO hole/electron pairs for each transition [2] further assist in characterising the Rydberg/valence character of the excited states.

More generally, study of the Rydberg-valence interaction in the excited states of small polyatomics, and how any valence character can evolve along specific coordinates, can help develop insight into a range of non-adiabatic processes in Rydberg excited states of small to medium sized polyatomic molecules [16].

2. Experimental apparatus and procedure

The absolute photoabsorption cross-sections of bz-imid and ph-imid were measured using the same equipment and procedure already described in relation to our work on imidazole [1]. Briefly, a cell incorporating LiF windows [17] was attached to a normal incidence monochromator [18] at the Daresbury Laboratory synchrotron radiation facility [19]. In the present experiment, a photon resolution of 0.1 nm FWHM (~ 5 meV at $h\nu = 8$ eV) was employed.

The photoabsorption cross-section was obtained through application of the Beer-Lambert law:

$$I_\text{t} = I_0 \exp(-n\sigma l) \tag{1}$$

where I_t is the intensity of the transmitted radiation after passing through the gas column, I_0 is the corresponding incident intensity, n is the gas number density, σ is the absorption cross-section and l is the length of the gas column. The absorption spectra of bz-imid and ph-imid were recorded at a temperature of $\sim 60°$ C, resulting in a sample vapour pressure of 8–10 μbar. The entire apparatus, comprising the cell, the sample and the baratron used to measure the sample pressure, was enclosed within an insulated box containing thermostatically controlled heating. This arrangement circumvented thermal transpiration effects [20]. The experimental uncertainty associated with the determination of absolute photoabsorption cross-sections using this cell is estimated as $\sim 5\%$ [21]. The photon energy scale was calibrated by recording high resolution spectra of a gas mixture comprising bz-imid (ph-imid), nitrous oxide and nitric oxide [21].

3. Computational details

All the calculations for benzene, ph-imid and bz-imid presented in this paper were performed at molecular equilibrium geometries found from a MP2/Aug-cc-pVTZ geometry optimisation. In the case of benzene, the calculated geometry obtained at this level ($r_\text{CC} = 1.394$ Å, $r_\text{CH} = 1.082$ Å) compares favourably with the experimental geometry ($r_\text{CC} = 1.397$ Å, $r_\text{CH} = 1.084$ Å) [22].

Excitation energies and excited state properties, including oscillator strengths, for the excited states of these molecules were obtained from frozen core CCSD coupled cluster calculations using the EOM formalism [23], principally as implemented in Q-Chem 5.4 [24]. A doubly augmented basis set, dAug-cc-pVTZ, was used for the benzene calculations to ensure sufficient diffuse functions for modelling the anticipated low-lying

Rydberg states, but because of the N^6 basis size scaling of the EOM–CCSD method this basis proved prohibitively expensive for the larger substituted imidazoles and consequently was reduced to the dAug-cc-pVDZ basis in these calculations. Previous imidazole calculations [1] were also now extended to this same EOM-EE-CCSD/dAug-cc-pVDZ level.

Subsequently, EOM-EE-CCSD(T) calculations were performed, again using Q-Chem [24], for all four molecules to obtain improved estimates of the vertical excitation energies. This is accomplished by a non-iterative perturbation treatment providing estimated corrections for the contribution of triply excited determinants in the coupled cluster treatment. In particular, we chose to use the recommended fT variant perturbation scheme for the excited states provided in Q-Chem [24] which uses the Hartree-Fock orbital energy difference for normalisation of the triples energy contribution. This does not, however, provide a balanced treatment of any additional correlation in the CCSD ground state reference and we omit any further ground state correction beyond the CCSD model. This focus on the excited state triples corrected energies may be justified since a primary objective for spectroscopic assignment is to obtain all excited state energies to comparable accuracy, and hence achieve a reliable estimation of *relative* excitation energies from the common ground state.

In what follows we will, for convenience, refer to these two levels of calculation simply as CCSD and CCSD(T).

The dAug-cc-pVTZ basis was retained for benzene but for the substituted imidazoles the N^7 scaling of the CCSD(T) treatment meant that even with the smaller d-Aug-cc-pVDZ basis the computational requirements exceeded the resources available. Hence, we adopted a more compact hybrid basis set (which we designate cc-pVDZ + R) consisting of un-augmented cc-pVDZ functions on the atomic centres with a large set of diffuse Rydberg-like functions placed at the molecular centre-of-mass. For the latter, we used the prescription of Kaufmann *et al.* [25] to generate a set of s, p, d, and f Rydberg-like functions ranging up to n = $5\frac{1}{2}$ ($n = 4\frac{1}{2}$ for f). We have previously benchmarked the performance of such a hybrid cc-pVXZ+R basis against the corresponding dAug-cc-pVXZ basis set in studies of fenchone [26] and α-pinene [27] and find that for calculating the low-lying Rydberg states (here 3p, 3s) the two basis sets yield nearly identical results. In the present work a further comparison of the performance of dAug-cc-pVDZ and cc-pVDZ+R EOM-CCSD calculations was made for these substituted imidazoles (see for example Supplementary Material, Table S1). This again reveals the equivalence of results from these two basis choices, but with the latter achieving a $> 25\%$ reduction in the number of basis

functions, with consequently significant computational savings.

Prior to commencing with the EOM-CCSD calculations, a preliminary investigation of the excited state landscape of ph-imid and bz-imid was made using more economical time-dependent density functional (TD-DFT) calculations. For these, the range-separated CAM-B3LYP functional was selected with the dAug-cc-pVTZ basis to help achieve the best estimation of Rydberg excited states by this method.

For both TD-DFT and CCSD calculations the identification/characterisation of the excited states was aided by visual examination of the NTOs [2]. These provide the simplest one-particle representation of an excitation using unitary transformations of the canonical HF orbitals to generate a single, or at least just a few, hole/electron orbital pairs that carry the transition amplitude. The leading hole/electron pair may thus be viewed as, respectively, the initial and final orbital in a one-electron promotion. Differences, $\Delta \langle R^2 \rangle$, between the excited and ground state spatial extents (second moments of the electron density) are further used to infer the diffuseness (Rydberg/valence character) of the excited state.

Vertical ionisation energies were estimated by Outer Valence Green's Function calculations (OVGF/cc-pVTZ). These results are reported in Table S2, Supplementary Material.

4. Results and discussion

4.1. Overview

The absolute photoabsorption cross-sections of bz-imid and ph-imid (present work), imidazole [1] and benzene [7], across the full energy range covered in this experiment, (4.4–10.8 eV), are plotted in Figure 1. The sharp structure observed in the absorption spectra of imidazole and much of that in benzene arises from transitions into Rydberg states belonging to series converging onto the relevant ionic ground state.

Figure 1 shows that the photoabsorption spectra of bz-imid and ph-imid exhibit some features which resemble those in the spectrum of benzene. For example, the spectrum of each molecule contains a prominent broad peak between 6.0 and 7.5 eV and another, much weaker, feature close to threshold. Similarly, the spectra of bz-imid, ph-imid and imidazole appear to contain some bands in common. For example, the broad bands around 5.3 eV in ph-imid and 6.0 eV in bz-imid seem similar to the band around 6.5 eV in imidazole. These spectroscopic similarities suggest that there may well be somewhat analogous electronic structure associated with
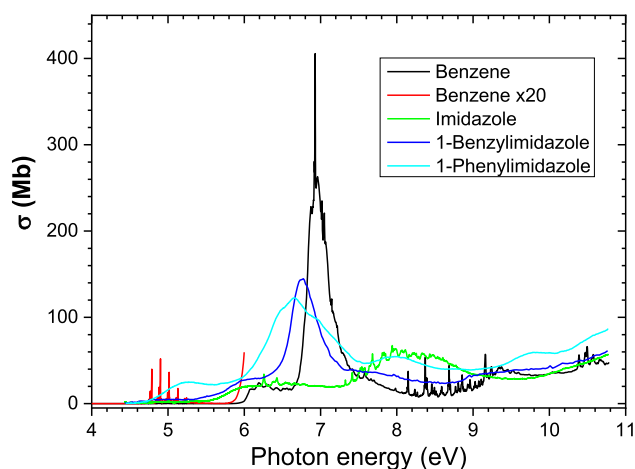
Figure 1. The absolute photoabsorption cross-sections, σ, of benzene [7], imidazole [1], benzylimidazole (present work) and phenylimidazole (present work).

these molecules. Plots of the highest occupied molecular orbitals of ph-imid and bz-imid are given in Figure 2 where similarities in the valence electronic structure of these two molecules are immediately obvious, with a majority of the outermost orbitals largely localised on either the imidazole or phenyl rings. Moreover, these localised orbitals are readily identified with the outer occupied valence orbitals in the isolated molecular rings, benzene and imidazole. (Plots of these latter orbitals are provided for convenience in the Supplementary Material as Figures S1 and S2, respectively.) The correspondence between the outermost six orbitals of ph-imid and bz-imid and those of either the benzene or imidazole constituent rings is collected and listed in Table 1. It should be noted, however, that the $C_5–N_4$ π density in the imidazole 3a'' HOMO orbital shifts to the $C_5–N_1$ position in the HOMOs of the substituted molecules (see Scheme 1 for numbering).

The ionisation energies (binding energies) of the outer orbitals in ph-imid and bz-imid are only slightly shifted compared to those of the corresponding orbitals in the separated component ring molecules (Table S2). This then underscores the likely parentage of the ph-imid and bz-imid occupied valence orbitals in terms of the isolated ring molecules, and our anticipation that transitions from these substituted imidazoles may display characteristics of the corresponding transitions in either benzene or imidazole. It should, however, be noted that analogous transitions to those that are symmetry forbidden in the highly symmetric benzene molecule become allowed in the absence of symmetry elements in the composite molecules ph-imid and bz-imid.

In assigning some of the absorption bands in imidazole [1], use was made of excitation energies estimated

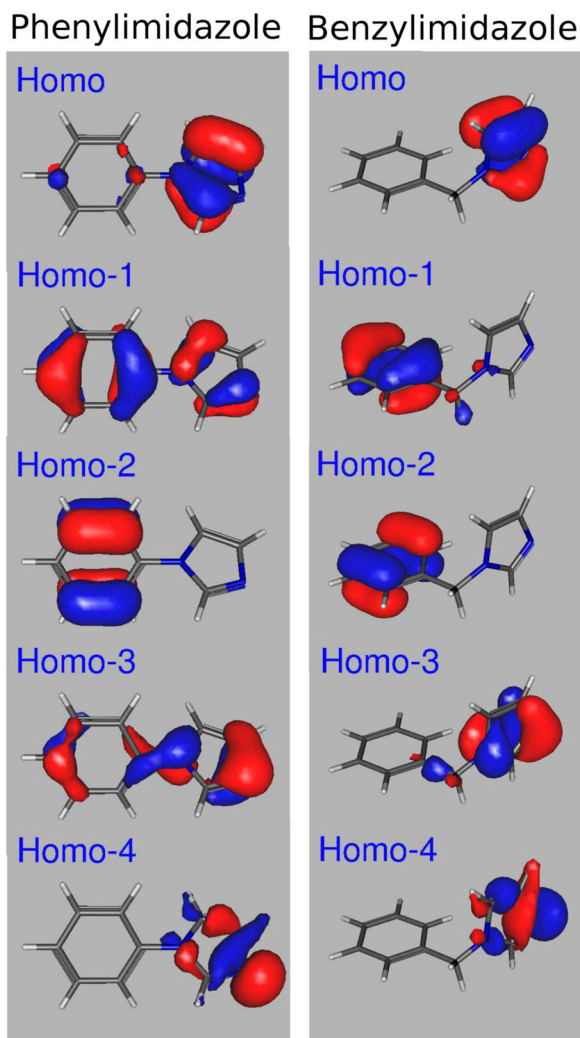## Phenylimidazole   Benzylimidazole

Figure 2. The outermost occupied valence orbitals, starting from the HOMO, of 1-benzylimidazole and 1-phenylimidazole, obtained from HF/cc-pVTZ calculations. (Corresponding plots of outer valence orbitals of benzene and imidazole may be found in Supplementary Material Figures S1 and S2.)

with experimentally derived quantum defects together with the known ionisation energy. Such procedures work well for isolated Rydberg states. However, our theoretical results for bz-imid and ph-imid indicate that most of the electronically excited states possess a mixed valence/Rydberg or Rydberg/Rydberg character. Hence, the assignments proposed for the absorption bands in bz-imid and ph-imid are based solely on our excited state calculations. These calculated results for the excited states of benzene, imidazole, ph-imid and bz-imid are summarised in Tables 2–5, respectively. Alongside the numerical results, a summary of the visual inspection of the principal hole/electron NTO pairings for each excitation is included in these tables. These are helpful in assessing the Rydberg, valence, or mixed Rydberg/valence character of the excited state and are further

discussed in the following sections. In the discussions below we will denote specific states by their sequence number, as it appears in the relevant table, preceded by #.

4.2. Benzene

The photoabsorption spectrum of benzene, in the energy range between threshold and the $\tilde{X}\ ^2E_{1g}$ state adiabatic ionisation energy of 9.243 eV [28], has been studied extensively [13,14]. A review of the early experimental work has been given by Robin [29] and many of the spectra are available in the MPI-Mainz UV/VIS Spectral Atlas [30]. The ground state molecular orbital configuration of benzene, in D_{6h} symmetry, is [28]

$$\dots (1a_{2u})^2(3e_{2g})^4(1e_{1g})^4(1e_{2u})^0(1b_{2g})^0\ ^1A_{1g}$$

Much attention has focussed on the valence π^* states due to the configurations

$$\dots (1a_{2u})^2(3e_{2g})^4(1e_{1g})^3(1e_{2u})^1(1b_{2g})^0\ B_{2u}, B_{1u}, E_{1u}$$
$$\text{and} \dots (1a_{2u})^2(3e_{2g})^4(1e_{1g})^3(1e_{2u})^0(1b_{2g})^1\ E_{2g}$$

In addition to these $\pi \rightarrow \pi^*$ valence excited states, transitions into Rydberg states may also occur. In the energy range relevant to the present work, these Rydberg states arise through excitation from the $1e_{1g}$ (HOMO) orbital. Thus, the Rydberg state symmetries are as follows: s (E_{1g}); p_z (E_{1u}), p_x, p_y (A_{1u}, A_{2u}, E_{2u}); d_{z^2}(E_{1g}), d_{xz}, d_{yz} (A_{1g}, A_{2g}, E_{2g}), $d_{x^2-y^2}$, d_{xy} (B_{1g}, B_{2g}, E_{1g}). For single photon absorption, in the D_{6h} point group, only transitions into states of A_{2u} or E_{1u} symmetry are allowed from an initial state of A_{1g} symmetry. However, structure associated with electric-dipole forbidden electronic states is observed in the single photon absorption spectrum of benzene due to additional excitation of non-totally symmetric vibrational modes (see refs [10–12] for a detailed discussion on this topic).

Our excited state calculations for benzene are summarised in Table 2. This includes the classification of the excited state character by a visual NTO analysis. States #1 and #2 are characterised as pure $\pi \rightarrow \pi^*$ valence excitations, and this is strongly supported by the calculated spatial extents which are barely increased from that of the ground state ($\Delta < R^2 > \approx 0$). Most other states are identified as Rydberg states that show steadily increasing $\Delta < R^2 >$ values, reflecting the increasingly diffuse nature of the Rydberg orbital. However, the NTO analysis ascribes a mixed Rydberg/valence character to states #6 and #8 and corroboration for this can be noted from their reduced spatial extents compared to those of adjacent pure Rydberg states.

Table 1. Approximate correspondence between molecular orbitals in phenylimidazole or benzylimidazole, and those in benzene or imidazole.

Molecular orbital	Orbital Number	Corresponding orbital in benzene or imidazole
Phenylimidazole		
HOMO	38	Imidazole HOMO (3a″) [a]
HOMO-1	37	Benzene HOMO ($1e_{1g}$) [b] (+ imidazole $p\pi$ orbitals)
HOMO-2	36	Benzene HOMO ($1e_{1g}$) [b]
HOMO-3	35	Imidazole HOMO-1 (2a″) + Benzene $p\pi$
HOMO-4	34	Imidazole HOMO-2 (15a′)
HOMO-5	33	Benzene HOMO-2 ($3e_{2g}$)
Benzylimidazole		
HOMO	42	Imidazole HOMO (3a″) [a]
HOMO-1	41	Benzene HOMO ($1e_{1g}$) [b]
HOMO-2	40	Benzene HOMO ($1e_{1g}$) [b]
HOMO-3	39	Imidazole HOMO-1 (2a″)
HOMO-4	38	Imidazole HOMO-2 (15a′)
HOMO-5	37	Benzene localised

[a] Note the imidazole 3a″ π orbital density at the $C_5 = N_4$ position shifts to the C_5-N_1 position in the substituted imidazole HOMOs.
[b] The degenerate $1e_{1g}$ HOMO pair in benzene is effectively split into doubly occupied HOMO-1 and HOMO-2 orbitals in the lower symmetry environment found in these substituted imidazoles.

Table 2. Benzene EOM–CCSD/dAug-cc-pVTZ excited state calculations of vertical excitation energies, spatial extents, $\langle R^2 \rangle$, and oscillator strengths, f, for dipole allowed transitions from the ground state. Also included are improved EOM-CCSD(T) energies applying a perturbative correction for triply excited determinants.

State		Excitation Energy (eV)			Oscillator Strength, f	% double substitution character, $(r_2)^2$	NTO Transition Character[c]
No.	Symmetry	CCSD	CCSD(T)[a]	$\Delta \langle R^2 \rangle$ (a_0^2)[b]			
11	$1B_{2g}$	7.75	7.47	104.6		6.4	$\pi \rightarrow d_{xy}, d_{x^2-y^2}$
10	$1B_{1g}$	7.74	7.46	101.6		6.4	$\pi \rightarrow d_{xy}, d_{x^2-y^2}$
9	$2E_{1g}$	7.62	7.34	62.5		6.2	$\pi \rightarrow d_{z^2}$
8	$2E_{1u}$	7.49	7.12	37.6	0.3364	6.8	$\pi \rightarrow p_z, \pi^*$
7	$1A_{1u}$	7.25	6.96	80.9		6.8	$\pi \rightarrow p_x, p_y$
6	$1E_{1u}$	7.21	6.88	45.7	0.3625	6.6	$\pi \rightarrow p_z, \pi^*$
5	$1E_{2u}$	7.16	6.87	75.8		6.5	$\pi \rightarrow p_x, p_y$
4	$1A_{2u}$	7.08	6.81	72.7	0.0618	6.1	$\pi \rightarrow p_x, p_y$
3	$1E_{1g}$	6.55	6.26	49.1		6.5	$\pi \rightarrow 3s$
2	$1B_{1u}$	6.48	6.08	4.0		5.9	$\pi \rightarrow \pi^*$
1	$1B2_u$	5.19	4.70	1.8		10.0	$\pi \rightarrow \pi^*$

[a] Difference of the excited state spatial extent (second moment of the electron density) from that of the ground state calculated at the same theoretical level. Here, a CCSD/dAug-cc-pVTZ calculation gives the ground state $\langle R^2_{Gnd} \rangle = 459.1\ a_0^2$.
[b] Vertical excitation including non-iterative corrections for triply excited determinants in the excited states, but omitting any corresponding CCSD ground state reference correction.
[c] Obtained by visual inspection of the principal pair of hole/electron Natural Transition Orbitals (NTOs) for the transition (Refs [2]). The z axis ($p_z\ d_{z^2}$) is the normal to the molecular plane.

While preparing an initial theory–experiment comparison from Table 2, it was noted that several of the key CCSD energies (states #1–#4, #6, #8) appeared ~ 0.3 eV too high. This discrepancy is at the upper end of the expected error (more typically 0.1–0.2 eV) at this level of computation for states that primarily result from a single electron promotion. However, the norm of the double excitation amplitudes, r_2^2 (listed in Table 2) for these CCSD excited states is around 6.5% (but rising to 10% for state #1). This degree of doubles character may indicate that the truncation of the cluster operator at doubly substituted determinants (as in CCSD) is too abrupt to fully capture correlation energy effects in the excited state. The description of these states can be most economically improved by a perturbation treatment of the

triples excitations that is added to the CCSD results for the excited states. Such improved excitation energies are included in Table 2 and are henceforth used as the basis for discussion.

A graphical comparison of the experimental absorption spectrum [7] and calculated oscillator strengths using the CCSD(T) corrected excitation energies is presented in Figure 3. The experimental vacuum ultraviolet (VUV) absorption spectrum is seen to be dominated by an intense structured peak observed around 7 eV. According to our CCSD(T)/dAug-cc-pVTZ theoretical predictions (Table 2), this peak arises from contributions associated with the three one-photon allowed 3p Rydberg transitions: $1e_{1g} \rightarrow 3p_{x,y}\ 1A_{2u}$ at 6.81 eV #4, $1e_{1g} \rightarrow 3p_z/\pi^*\ 1E_{1u}$ at 6.88 eV #6 and $1e_{1g} \rightarrow 3p_z/\pi^*\ 2E_{1u}$ at

Table 3. Imidazole excited state predictions. EOM–CCSD/dAug-cc-pVDZ calculations of vertical excitation energies, oscillator strengths and size for singlet excited states.

State No.	Sym.	CCSD Energy (eV)	Oscillator Strength f	Spatial Extent [a] $\Delta < R_\chi^2 >$ (a_0^2)	CCSD(T) Energy (eV) [b]	Natural Transition Orbitals Initial	Final [c]
20	A′	7.87	0.0183	188.7	7.66	3a″	$4p_z$
19	A′	7.82	0.0051	71.7	7.67	15a′	$[\sigma_{CH}]/p_{x/y}$
18	A″	7.79	0.0005	275.0	7.59	3a″	'$4p_{xy}$'
17	A′	7.75	0.0263	64.9	7.60	15a′	$[\sigma_{CH}*/\sigma_{NH}*]/p_{x/y}$
16	A″	7.69	0.0059	280.1	7.50	2a″	$p_{x/y}$
15	A′	7.53	0.0106	108.4	7.30	3a″	$[C=C\pi]/d$
14	A″	7.44	0.0000	216.2	7.24	3a″	$[\sigma_{NH}]/$ 'Rydberg'
13	A′	7.39	0.0083	112.7	7.19	3a″-like	d
12	A″	7.31	0.0031	99.3	7.10	3a″	d
11	A″	7.15	0.0026	92.8	6.93	3a″	d
10	A′	7.11	0.1005	35.0	6.84	3a″ + 15a′	$[\sigma_{NH}*]s + \pi*$ '$3p_z$'
9	A′	7.03	0.0024	35.6	6.79	15a′	$s/\sigma_{NH}*$
8	A″	7.01	0.0007	59.2	6.78	3a″	d
7	A″	6.92	0.0022	10.9	6.60	15a′	$\pi*$
6	A″	6.89	0.0046	35.5	6.69	2a″	$3p_z/\sigma_{NH}*$
5	A′	6.81	0.0047	27.2	6.46	π (similar to HOMO)	$3p_z/\pi_{C-N-C=N}*$
4	A″	6.58	0.0005	64.3	6.37	3a″	$3p_y$
3	A′	6.40	0.1194	35.9	6.10	3a″	$3p_z/\pi_{C-C-N}*$
2	A″	6.36	0.0271	61.7	6.15	3a″	$3p_x/[\sigma_{CH}*/\sigma_{NH}*]$
1	A″	5.60	0.0006	41.0	5.36	π (similar to HOMO)	$3s/[\sigma_{NH}*]$

[a] Difference of the excited state spatial extent (second moment of the electron density) from that of the ground state calculated at the same theoretical level. Here, a CCSD/dAug-cc-pVTZ calculation gives the ground state $\langle R_{Gnd}^2 \rangle = 287.03\ a_0^2$.

[b] Vertical excitation including non-iterative corrections for triply excited determinants in the excited states, but omitting any corresponding CCSD ground state reference correction.

[c] Excited state character denoted, as appropriate, in terms of Rydberg and valence contributions. Relatively weak contributions to the overall final state character are denoted by inclusion within square brackets []. Ambiguous or uncertain descriptions are enclosed between single quotes.

7.12 eV #8. These excitation energies are broadly in line with previous calculations [8], although lying ~ 0.1 eV to lower energy. There is, however, no clear consensus in the literature on individual assignments to noted experimental features [4,14] in this band, although Hiraya and Shobatake [6] assign a feature at 6.87 eV in their jet cooled spectrum to an E_{1u} state origin. While they list this as the $2E_{1u}$ state, this numbering relies on very tentative attribution of nearby lower energy structure to the $(1E_{1u} + 1B_{1u})$ transitions; these calculations suggest it should be assigned as the $1E_{1u}$ transition. (It may be noted that, as the triples CCSD(T) correction is non-variational, the energetics are not constrained to be an *upper* estimate.)

The influence of Jahn–Teller effects on the vibronic structure in these 3p Rydberg states in benzene has been investigated previously [31].

The absorption bands associated with the nominally one-photon forbidden $1B_{2u}$ and $1B_{1u}$ states, arising from the $1e_{1g} \rightarrow 1e_{2u}$ valence transition, are mentioned only briefly. Our vertical excitation energies of 4.70 and 6.08 eV for the $1B_{2u}$ #1 and $1B_{1u}$ #2 states, are in reasonable agreement the experimental values of 4.9 and 6.2 eV [6]. The vibronic structure associated with these states has been discussed previously [11,12]. Above these two valence transitions we anticipate the first Rydberg state, #3, arising from the $1e_{1g} \rightarrow 3s\ 1E_{1g}$ transition, with a calculated excitation energy of 6.26 eV (Table 2). An

adiabatic 3s excitation energy of 6.334 eV was measured by Johnson in a $(2+1)$ REMPI study [26].

Turning attention to the remaining Rydberg states predicted in Table 2, the lowest energy d-type Rydberg state excitation is the $1e_{1g} \rightarrow 3d_{z^2}\ 2E_{1g}$ #9 transition, with a calculated vertical excitation energy of 7.34 eV. The origin of this state has been observed at 7.535 eV in a REMPI study [28] and at 7.435 eV in an electron impact investigation [9]. Our calculated vertical excitation energies for the $1e_{1g} \rightarrow d_{x^2-y^2}$, $d_{xy}\ 1B_{1g}$ and $1B_{2g}$ transitions are 7.46 eV #10 and 7.47 eV #11. An excitation energy of 7.449 eV has been estimated for the $1B_{1g}/1B_{2g}$ states [30].

Overall, our theoretical predictions provide a satisfactory description of the valence shell electronically excited states of benzene up to an energy of ~ 8 eV and allow an interpretation of the major features appearing in the photoabsorption spectrum (Figure 3).

4.3. Imidazole

The valence shell photoabsorption spectrum of imidazole has been studied recently by Holland *et al.* [1]. For the current work, the previous theoretical calculations for imidazole excited states have been complemented by a new EOM-CCSD(T) calculation to provide consistent levels of treatment for the excited states in all four molecules to be discussed (benzene, imidazole, phenyl-

Table 4. Phenylimidazole excited state energy calculations, including oscillator strengths, f, and relative spatial extents, $\Delta\langle R^2\rangle$.

| | TD-DFT(CAM-B3LYP)/dAug-cc-pVTZ | | | EOM–CCSD/cc-pVDZ+R | | | | CCSD(T)[c] | Initial | CCSD NTO Pair Analysis [e] | |
	E (eV)	f	$\Delta\langle R^2\rangle$ (a$_0^2$)[a]	E (eV)	f	$\Delta\langle R^2\rangle$ (a$_0^2$)	$(r_2)^{2b}$	E (eV)	Orbital [d]	Initial	Final
25				7.25	0.0279	180.4	6.8	6.99	H, (H-2)	H (Im π)	ΦI d
24				7.23	0.0570	172.4	7.2	6.98	H-2	Im π [Bz π]	ΦI d
23				7.23	0.0595	101.9	7.2	6.96	H-1	Im π Bz π	ΦI d
22				7.15	0.1431	137.7	7.4	6.85	H	H (Im π)	ΦI 'd'
21				7.08	0.2669	84.8	7.7	6.73	H, H-2	Im π (Bz π)	ΦI π: 'd'
20				7.06	0.0226	122.0	7.5	6.74	H	H (Im π)	[ΦI π] : ΦI 'd'
19				7.05	0.0279	131.7	7.4	6.76	H, H-1	Im π (Bz π)	ΦI d
18				6.96	0.0394	83.4	7.3	6.64	H	H (Im π)	Bz π*: ΦI d
17				6.92	0.1615	38.3	8.4	6.52	H-1, H-2	Bz π Im π	Bz π*: ΦI d
16				6.90	0.1200	62.0	7.4	6.58	H, H-1, H-2	Bz π Im π	ΦI d
15	6.78	0.0453	56.9	6.85	0.0245	68.9	7.3	6.55	H-1	Bz π Im π	Im π Bz π: p
14	6.77	0.1671	56.8	6.74	0.0060	81.3	7.0	6.47	H, H-1	Bz π Im π	ΦI p
13	6.74	0.1989	36.9	6.74	0.0071	64.7	7.2	6.47	H-1, H-2	Bz $1e_{1g}$ π	Bz s
12	6.63	0.0027	86.4	6.70	0.0046	61.5	7.4	6.42	H-1, H-2	Im π Bz π	Im π*: Bz s/p
11	6.54	0.2963	14.8	6.66	0.0105	43.5	7.7	6.32	H, H-1, H-2	Im π Bz π	Im π (Bz π): ΦI 'd'
10	6.45	0.1415	45.3	6.60	0.0114	83.4	7.4	6.31	H, [H-1]	H (Im π)	ΦI p
9	6.42	0.2	19.5	6.56	0.0017	−8.2	9.7	6.14	H-4, [H-3]	Im H-2 σ	Im pπ
8	6.29	0.0258	42.5	6.45	0.0293	46.9	8.0	6.08	H	H (Im π)	Bz π*: ΦI p_3
7	6.26	0.0015	21.1	6.38	0.0252	26.1	9.0	5.93	H	H (Im π)	Bz π*: ΦI p_2
6	6.22	0.0164	14.9	6.28	0.0007	38.5	8.0	5.91	H	H (Im π)	Bz π*: ΦI p_1
5	5.91	0.0034	38.5	6.17	0.0063	58.9	7.0	5.91	H-1, (H)	Bz π [Im π]	Bz s
4	5.82	0.0108	8.7	6.13	0.1161	7.3	8.2	5.69	H-1, (H)	Im π [Bz π]	ΦI π*
3	5.70	0.1009	2.1	5.82	0.0109	44.9	6.8	5.54	H	H (Im π)	ΦI s
2	5.31	0.1489	0.9	5.68	0.1864	0.7	8.8	5.21	H	Im π [Bz π]	ΦI π*
1	5.13	0.0039	−0.3	4.97	0.0012	−1.2	10.5	4.51	H-1, H-2	Bz $1e_{1g}$ π	Bz π*

[a] Difference of the 2nd moment of the electronic state density, $\langle R^2\rangle$, from that of the ground state, $\langle R_{Gnd}^2\rangle$, calculated at the same theoretical level: for CAM-B3LYP $\langle R_{Gnd}^2\rangle = 1826.0$ a$_0^2$; for CCSD $\langle R_{Gnd}^2\rangle = 1836.6$ a$_0^2$.
[b] The % degree of doubles substitution in the CCSD wavefunction.
[c] Vertical excitation with EOM–CCSD(fT) corrected energy for the excited state, but omitting any corresponding ground state correction.
[d] Initial ph-imid canonical orbital in the leading transition amplitude to the excited state.
[e] Condensed descriptions of the principal NTO pair. Bz, Im indicate a localisation (centering) of valence (Rydberg) orbitals at a specific ring; alternatively, ΦI is used to denote NTO orbitals that are either centred midway between the two ring structures or delocalised over the whole molecule. For those NTO orbitals judged to be analogous to a canonical orbital of phenyl-imidazole H, H-1 are used to indicate a HOMO, HOMO-1 etc. Parentheses () are used to show an approximate equivalence while [ ] are used to indicate a significant minor contribution to the transition amplitude. Ambiguous or uncertain descriptions are enclosed within single quotes.

and benzyl-imidazole). The EOM/CCSD(T) results up to state #20 are presented here in Table 3, and may be directly compared with our earlier TD-DFT imidazole results which may be found in Table 1 of Ref. [1].

To facilitate discussion on the electronically excited states in ph-imid (section 4.4) and bz-imid (section 4.5), the absorption spectrum of imidazole, up to an energy of 9.0 eV, is plotted in Figure 4. For comparison, the CCSD(T) excitation energies from Table 3 are added into the plot as a stick spectrum. As for benzene, an explicit correction for the ground state's triply excited determinants is omitted from these numerical results, and instead they are plotted with an empirically determined constant -0.125 eV offset to allow best comparison of the relative separation energies of the states. Additionally, it was now possible to extend the CCSD(T) results to more highly excited states, spanning energies up to 8.5 eV. An overview of these additional EOM-CCSD(T) calculations is provided by their inclusion in the stick spectrum in Figure 4, and the extended numerical results may be found in Table S3, Supplementary Material.

While these new EOM-CCSD results reveal some deficiencies in the more economical TD-DFT calculation, the previous assignment did not rely only on these calculations. For transitions into Rydberg states, the vibrational structure appearing in the photoabsorption spectrum was compared to that observed in the $\tilde{X}\ ^2$A" state photoelectron band [15] and Rydberg structure was identified using excitation energies estimated using quantum defect analyses. In general, the assignments for the imidazole spectrum proposed by Holland *et al.* [1] are not substantially affected by the availability of these new calculations.

4.4. Phenylimidazole

Two sets of theoretical calculations, by TD-DFT and coupled cluster methods, are shown in Table 4. A quick way to obtain an overview of these theoretical predictions is to plot them as spectral simulations, by folding the stick spectra (energy vs. oscillator strength) with a Gaussian broadening function to generate a realistic profile for comparison with experiment. These are shown in

Table 5. Benzylimidazole excited state energy calculations, including oscillator strengths, f, and relative spatial extents, $\Delta \langle R^2 \rangle$.

| | TD-DFT(CAM-B3LYP)/dAug-cc-pVTZ | | | EOM–CCSD/cc-pVDZ+R | | | | | | CCSD NTO Pair Analysis [f] | |
	E (eV)	f	$\Delta \langle R^2 \rangle$ $(a_0{}^2)^a$	E (eV)	f	$\Delta \langle R^2 \rangle$ $(a_0{}^2)^b$	$(r_2)^{2c}$	CCSD(T)[d] E (eV)	Initial Orbital [e]	Initial	Final
20				7.08	0.0542	89.6	7.2	6.81 [g]	H, H-1, H-2	BI π	Bz π*: 'd'
19				7.06	0.0177	114.5	7.0	6.78	H	H (Im π)	d
18				7.05	0.0578	91.1	7.0	6.79	H, H-2	BI π	d: [Bz π*]
17				7.00	0.0875	78.2	6.9	6.72	H, (H-1), H-2	BI π	Bz π*:BI d [p]
16				6.98	0.0246	68.2	7.4	6.69	H, H-1	BI π	Bz p: 'd'
15	6.83	0.4637	8.4	6.97	0.0154	80.9	6.8	6.72	H, H-1	BIπ (Bzπ + Im 3a''π)	BI d [Im π]
14	6.82	0.1087	39.0	6.93	0.0023	74.4	7.5	6.66	H, H-1, H-3	H + H-1 (Bzπ + Im π)	BI p, 'd'
13	6.74	0.0746	35.1	6.89	0.0604	64.0	7.5	6.56	H	H (Im π)	Im pπ*: 'p'
12	6.69	0.1148	25.0	6.87	0.0081	7.7	8.9	6.53	H-4	Im 15a' σ	Im pπ*
11	6.61	0.0429	39.4	6.83	0.0364	60.9	7.6	6.51	H, H-1	H-1(Bzπ) + Im 3a''π	Bz 1e$_{2u}$ π*: p/'d'
10	6.59	0.0113	−17.9	6.75	0.0088	57.7	7.4	6.45	H	H (Im π)	BI 'd': Bz π*
9	6.54	0.0045	49.1	6.64	0.005	45.0	7.9	6.33	H, (H-3)	H (Im π)	'd': [BI pπ*]
8	6.45	0.0111	36.7	6.56	0.0032	45.3	7.5	6.27	H-2, (H)	H-2(Bzπ) [Imπ]	Bz 3s: BI 'd'
7	6.39	0.0064	41.7	6.51	0.0251	41.6	6.5	6.21	H-1, H-2, (H)	H + H-1 (Bzπ + Imπ)	Bz 1e$_{2u}$ π*: Bz 'p'
6	6.23	0.1092	−5.5	6.47	0.0007	36.0	6.8	6.16	H, H-1, H-2	H + H-1 (Bzπ + Imπ)	Bz 1e$_{2u}$ π* : BI 'p'
5	6.14	0.0369	−1.5	6.36	0.0006	57.2	6.8	6.12	H-1, (H)	Bz 1e$_{1g}$ π	Bz 3s
4	6.05	0.0334	0.2	6.25	0.0254	42.3	7.0	5.96	H	H (Im π [Bz π])	BI 'p'
3	5.93	0.0071	−5.3	6.17	0.0374	43.7	7.0	5.88	H	H (Im π)	Im 3p
2	5.80	0.0231	17.3	5.81	0.0132	48.1	6.6	5.55	H	H (Im π)	Im 3s
1	5.36	0.0025	−16.9	5.17	0.0007	0.2	10.3	4.75	H-1, H-2	Bz 1e$_{1g}$ π	Bz 1e$_{2u}$ π*

[a] Difference of the spatial extent (second moment of the electron density) from that of the ground state obtained from a B3LYP/dAug-cc-pVTZ calculation, $\langle R^2_{Gnd} \rangle = 2260.2\ a_0{}^2$.

[b] Difference of the spatial extent from that of the CCSD/cc-pVDZ + R ground state calculated $\langle R^2_{Gnd} \rangle = 2244.2\ a_0{}^2$.

[c] The % degree of doubles substitution in the CCSD wavefunction.

[d] Vertical excitation with EOM–CCSD(fT) corrected energy for the excited state, but omitting any corresponding ground state correction.

[e] Initial ph-imid canonical orbital in the leading transition amplitude to the excited state.

[f] Condensed descriptions of the principal NTO pair as explained for Table 3. Here BI is used to denote NTO orbitals that are either centred midway between the two ring structures or delocalised over the whole molecule.

[g] We were unable, for technical reasons, to calculate a Triples correction in this case, and so this value was estimated from the observed correlation between $(r_2)^2$ and the correction terms calculated for the other states.
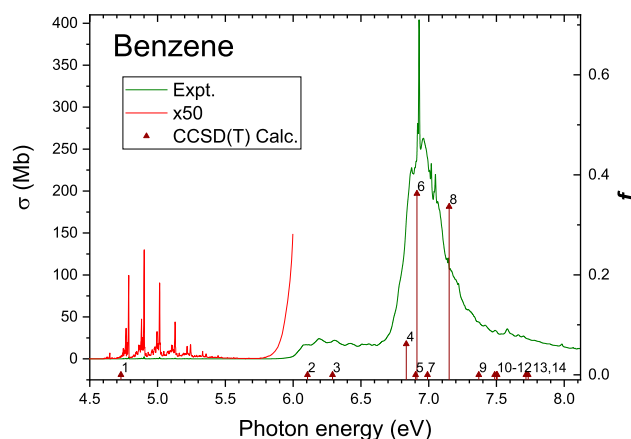

Figure 3. CCSD/dAug-cc-pVTZ predictions for electronic transitions of benzene and the experimental single-photon absolute absorption cross-sections, σ, from [7]. The calculated excited states are numbered as specified in Table 2 and are shown for both single-photon allowed (oscillator strength $f > 0$) and for single-photon forbidden ($f = 0$) transitions. The state excitation energies are from the CCSD(T) calculation incorporating non-iterative triples corrections and are plotted with an additional +0.03 eV energy offset to best align with experiment.

Figure 4. The single-photon absorption spectrum of imidazole showing the absolute absorption cross-section, σ (data taken from Ref. [1]). This is compared with the theoretically predicted vertical electronic transitions with oscillator strengths obtained by EOM–CCSD/dAug-cc-pVDZ calculations, with excitation energies obtained at the CCSD(T) level (Table 3). These values have been plotted with a -0.125 eV offset to best align with experiment.

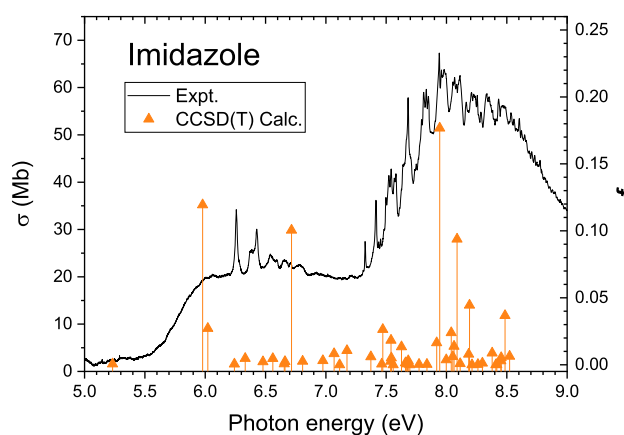Figure 5 together with the experimental absorption spectrum. The TD-DFT simulation reproduces the experiment seemingly well, including perhaps the very weak inflection at 5.7 eV. Note that because the calculation of states is truncated at ~ 7 eV the folded simulation is expected to fall too rapidly to high energy of the main absorption band.
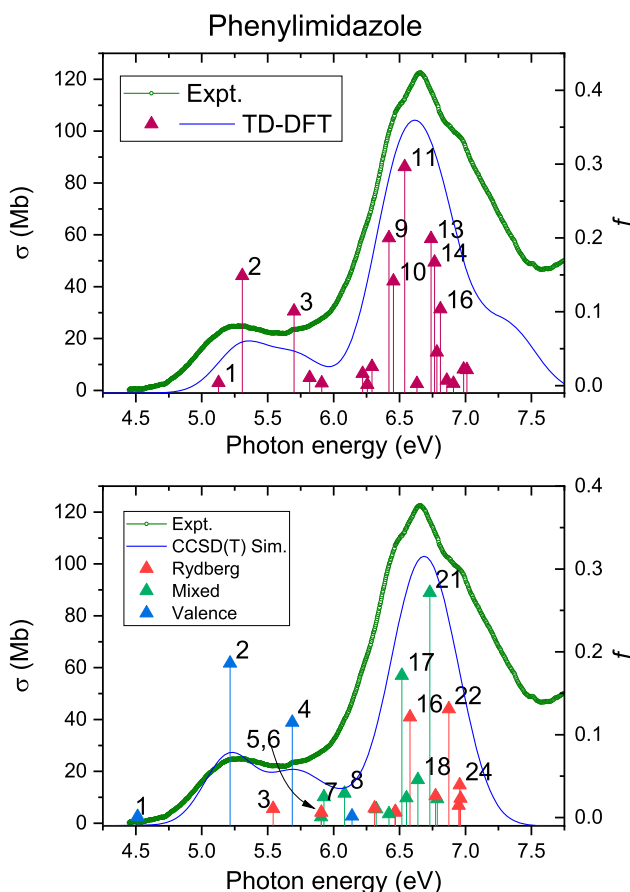
Figure 5. Experimental absolute photoabsorption cross-section, σ, of phenylimidazole. The theoretical simulations of the spectrum are prepared by folding the calculated stick spectrum (energy vs. oscillator strength, f) with a Gaussian broadening function, here arbitrarily chosen as 450 meV FWHM in order to achieve a realistic profile for the comparison. The top panel shows the CAM-B3LYP/dAug-cc-pVTZ calculations while the lower panel contains the CCSD(T)/cc-pVDZ+R results. The individual CCSD calculated transitions have been colour coded to indicate a broad classification as either Rydberg, valence, or mixed excitations by inspection of the NTO results (Table 4). For clarity only the more intense predicted transitions are numbered in the plots.

When following the same procedure for the CCSD simulation it became apparent that the generated spectral profile sat around 0.4 eV too high in energy. This is analogous to the situation encountered with the CCSD results for benzene, discussed in section 4.2. The percentage of double substituted character in the ph-imid CCSD wavefunction is included in Table 4 and can be seen to range from ∼7 to 10.5%. As was done with benzene, the excitation energies were recalculated at the CCSD(T) level, including a perturbation treatment for triple excitations in the excited states in an effort to better capture electron correlation effects, and these are used for the energies in the coupled cluster stick spectrum and simulation in Figure 5. (The correlation

between the triples energy correction and the norm of the double substitution amplitudes in the CCSD calculation is examined in the Supplementary Material, Figure S3).

Despite the TD-DFT and CCSD(T) simulations generating profiles matching the experimental spectrum equally well, there are clear discrepancies at the level of the stick spectra. The two prominent transitions seen below 6 eV (Figure 5) that define the relative absorption intensity predicted below the principal 6.7 eV peak are in good agreement; the different numbering of the 5.7 eV excitation is rather trivially explained by the energetic ordering of states #3, #4, #5 in the TD-DFT calculation; state #5 evidently corresponds to state #3 in the CCSD results, most clearly seen by comparing the $\Delta\langle R^2\rangle$ values (Table 4) in this region. Hence, the TD-DFT state #3 corresponds to CCSD state #4 etc.

Underneath the main experimental peak at 6.7 eV the situation is much more complex. While the pattern of the most intense quartet of coupled cluster peak predictions — #17 #16 #21 #22 — is echoed in the TDDFT spectrum — #9 #10 #11 #13/14 — the numbering discrepancy suggests there are missing states in the TD-DFT calculation. The ionisation energies of the five outermost orbitals in ph-imid span an energy range of less than 2 eV (Table S2) so Rydberg states belonging to series converging onto these limits would be expected to overlap significantly. It is also apparent that resultant congestion in the experimental spectrum precludes resolving discrepancies between the calculations by a more direct theory–experiment comparison.

TD-DFT has well-documented shortcomings when calculating charge transfer and Rydberg states, although we have tried to ameliorate these by using the CAM-B3LYP range separated hybrid functional [32]. Nevertheless, the ph-imid excited states include both Rydberg and valence charge-transfer character, and so is a priori a challenge for TD-DFT. Of perhaps greater concern, while TD-DFT inherently includes differential correlation effects through the correlation functional, it is a single reference method restricted to description of single-excitations. Since the CCSD results indicate a significant role for double excited determinants in ph-imid, the reliability of TD-DFT is clearly in question. It may be noted (Table 4) that the excitation energy for state #1, a $\pi \rightarrow \pi^*$ transition, is given as 5.13 eV by TD-DFT, but 4.97 eV in the CCSD calculation (with an indicated 10.5% doubles character) and falls further to 4.51 eV with the CCSD(T) perturbation treatment of triply excited determinants. The following discussion is therefore framed in terms of the CCSD results (together with the CCSD(T) corrected excitation energies) in Table 4, as these are likely to be the more reliable for detail,
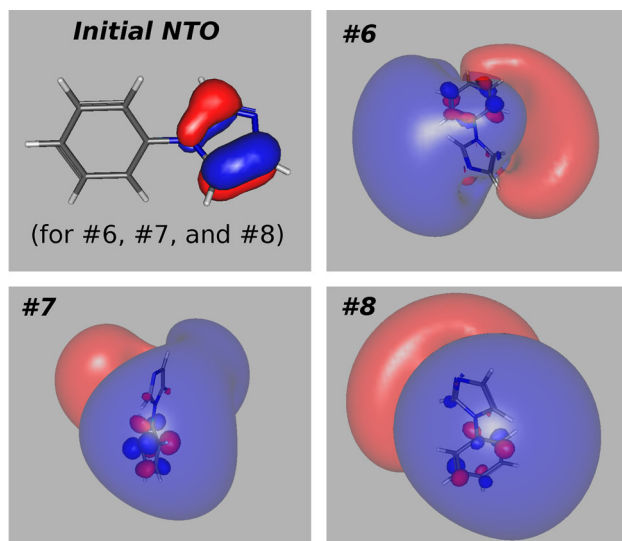
Figure 6. Phenylimidazole NTO plots for the excited states #6–#8. The top left panel shows the initial NTO for these transitions. These initial orbital plots are indistinguishable for the three transitions considered. The remaining panels are three-dimensional plots for the labelled excited states. These reveal the inner orbital pπ structure on the phenyl ring which is rendered as an opaque iso-surface (value 0.035). In these plots, the more diffuse Rydberg p character appears as a transparent iso-surface (value 0.005). Note the imidazole $\rightarrow$ phenyl ring shift of the valence electron density.

Figure 7. Phenylimidazole NTO plots for the excited states #18 and #22. The upper panels display a transparent isosurface (value 0.005) revealing the diffuse Rydberg d character of these states. The #18 plot includes an inner, opaque surface (value 0.04) that reveals its valence pπ structure around the phenyl ring. Contour plots of the electron density are provided in the lower panels. For state #18 the contour plot has been constructed in a plane midway along, and normal to, the C-C bond connecting the phenyl and imidazole rings – that is approximately the central horizontal plane, above the phenyl ring, in the upper 3-dimensional rendered plot. The plane of the #22 contour plot contains the C-C bond interconnecting the two ring systems and lies midway between planes that are normal to the phenyl- and to the imidazole rings. In both cases, the plot region extends ± 22 a_0 along each axis.

despite the apparently successful replication by the TD-DFT calculations of the overall experimental spectrum profile.

Considering then the characterisation of the ph-imid excited states, a first notable feature is the relatively small increase (even decrease), in the size of the excited states #1, #2, #4, and #9 compared to that of the ground state (indicated by the $\Delta\langle R^2\rangle \leq 7$ a.u. predictions in Table 4). One may immediately infer these states to be valence excitations. Conversely, the remaining states predicted to have larger $\Delta\langle R^2\rangle$ must correspond to excitations having a significant Rydberg character. From the NTO analysis, states #3, #5 and #13 can be classed as 3s Rydberg states (albeit having different molecular ion cores); states #10 and #14 are p-type Rydbergs. The $\Delta\langle R^2\rangle$ values for these essentially pure Rydberg states increase steadily from 45 to 83 a.u. Falling energetically between these s and p Rydberg states are the mixed Rydberg valence states #6—#8 and these have correspondingly reduced $\Delta\langle R^2\rangle$ values, that fall between the pure s and p Rydberg values. Figure 6 shows the excited NTO plots of the mixed states #6—#8, and Figure 7 plots the orbital density of the mixed Rydberg–valence state #18 and pure Rydberg state #22. Other example ph-imid NTO plots may be found in the Supplementary Material.

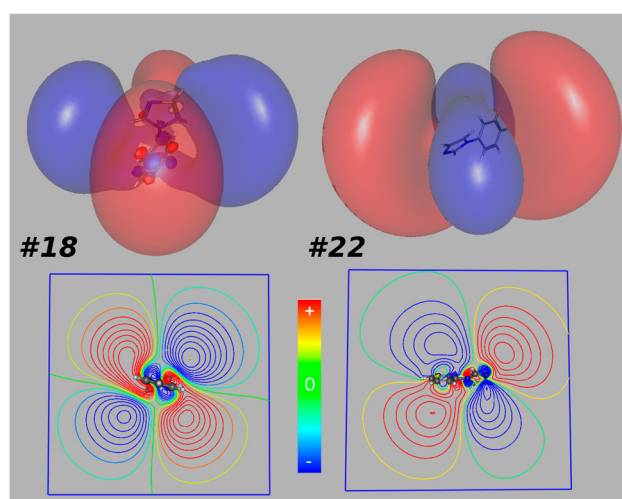We now return to a comparison of the more significant of these theoretically predicted states with the experimental spectrum (Figure 5). The state #1 transition, with a predicted CCSD(T) excitation energy of 4.51 eV, is firmly localised on the phenyl ring and is clearly analogous to the lowest energy $1e_{1g} \rightarrow 1e_{2u}$ $1B_{2u}$ transition in benzene (experimental value of 4.9 eV [6]). In D_{6h} benzene this transition only becomes allowed by vibronic interaction, and while in the non-symmetrical ph-imid the electronic transition is no longer symmetry forbidden it has a very low predicted oscillator strength. Consequently, it is no surprise that the calculated transition falls in the very weak pedestal at the onset of the experimental spectrum.

The second calculated excitation of state #2 is a transition to a pure valence pπ NTO extending across the whole ph-imid molecule. It coincides with the first weaker band, peak ~ 5.25 eV, in the experimental spectrum. Perhaps because of the valence character, it has a large oscillator strength, whereas the next state #3, an excitation from the same imidazole localised π orbital but now to a pure 3s Rydberg state is predicted to be an order of magnitude weaker transition and cannot be discerned in the experimental spectrum. In imidazole the

first excitation is of the 3s Rydberg falling at the weak absorption onset around 5.5 eV.

State #4 is another pure valence state, this time the result of a transition from an imidazole π orbital that is now partially delocalised to include density around the phenyl ring, into a ph-imid wide pπ structured orbital. Its predicted CCSD(T) energy of 5.69 eV seems to coincide with a weak inflection that appears in the experimental spectrum (Figure 5) below 6 eV. State #5 is a second 3s Rydberg excitation (albeit with a different molecular ion core) but again is expected to be too weak to significantly influence the appearance of the experimental spectrum.

The mixed Rydberg–valence states #6, #7, #8 (shown in Figure 6) have in common a transition from an imidazole ring localised π orbital to one of the triple 3p Rydberg orbitals, analogous to the 3a'' excitations #2, #3, #4 in imidazole (Table 3). In both molecules these have also mixed valence character and calculated energies 5.91–6.08 eV (ph-imid) and 6.15–6.37 eV (imidazole). In the imidazole spectrum (Figure 4) two of these states are particularly intense and hence prominent; in the ph-imid spectrum (Figure 5) the transitions #7 and #8, though less prominent, may nevertheless importantly contribute intensity in the valley between the two principal bands.

A particularly interesting feature of the ph-imid states #6–#8 (Figure 6) is that the non-Rydberg part of the excitation to a phenyl ring localised pπ orbital, can be considered a π–π charge transfer process from an imidazole ring donor to a phenyl ring acceptor within the molecular ion core.

The remaining excitations listed in Table 4 fall under the broad peak centred at 6.6 eV, with states #16, #17, #21 and #22 being particularly prominent. The calculated CCSD(T) excitation energies of #16 and #17, respectively 6.58 and 6.52 eV, suggest that these two states may be associated with the shoulder evident at $\sim$6.5 eV in the experimental spectrum (Figure 5), to low energy of the peak maximum. Both are characterised by the NTO analysis as excitations from a pπ orbital structure extending over the full molecule to d-type Rydbergs, but while #16 is a pure Rydberg state, state #17 displays a mixed Rydberg–valence (phenyl ring pπ orbital) character resembling the benzene 1e$_{2u}$ virtual orbital. Hence the valence part of this latter transition is loosely analogous to the one-photon allowed 1e$_{1g}$ → 1e$_{2u}$ E$_{1u}$ #6 transition in benzene (Table 2). Both are predicted as relatively strong transitions contributing intensity to the main experimental features in the respective absorption spectra.

The next transition, to state #18, is predicted to lie directly beneath the large peak in the absorption spectrum but because of a weaker oscillator strength plays a less prominent role in the simulation (Figure 5) than the immediately preceding states. Like #17, the excited state is predicted to have mixed Rydberg–valence character (see Figure 7), the latter arising as another phenyl pπ structure, but unlike #17 the initial NTO 'hole' is localised on the imidazole ring and resembles the imidazole 3a'' HOMO. Hence, like states #6–#8, the valence contribution to the state #18 transition can be viewed as a π–π charge transfer process from an imidazole ring donor to a phenyl ring acceptor.

The strongest transition in the region being investigated is #21, whose calculated excitation energy of 6.73 eV is close to the experimental peak maximum 6.65 eV. From the simulation (Figure 5) it is clear that this transition significantly influences the appearance of the absorption peak. The transition to #21 is evidently complex and cannot be captured by just a single NTO transition pair. Nevertheless, a reasonable description appears to have a transition from an initial pπ structured orbital on both the imidazole and, to a lesser extent, the phenyl rings leading to a mixed state with pπ valence character distributed over the full ph-imid molecule plus a more diffuse character that only approximately resembles a hydrogenic d orbital. These characteristics suggest a unique ph-imid transition, with no close analogy in either benzene or imidazole.

The last intense transition is that of #22. Its predicted excitation energy of 6.85 eV closely aligns with the $\sim$6.9 eV shoulder on the side of the absorption spectrum (Figure 5), inviting an assignment of this experimental feature. From our calculation the transition #22 arises from the ph-imid HOMO, resembling the imidazole 3a'' HOMO, to a pure d Rydberg (see Figure 7). The analogous 3a'' → d Rydberg transition in imidazole (#8) has a CCSD(T) calculated excitation energy of 6.78 eV (Table 3)

4.5. Benzylimidazole

Our calculated results for bz-imid are presented in Table 5, and as in the preceding discussion of ph-imid, simulated spectra have been prepared by generating stick spectra (energy vs. oscillator strength, f) which are then folded with a broadening function. These simulations are compared with experiment in Figure 8. While the profiles of the TD-DFT and coupled-cluster calculations appear equally good in comparison with experiment, at the level of individual transitions there are clear discrepancies between the methods with potentially missing states in the TD-DFT results. A priori, the coupled cluster approach can be preferred as the likely more reliable. In the coupled-cluster CCSD calculations the norm of the amplitude vectors for double substitutions again ranges between 6.5% and 10.3%, signalling a need to improve
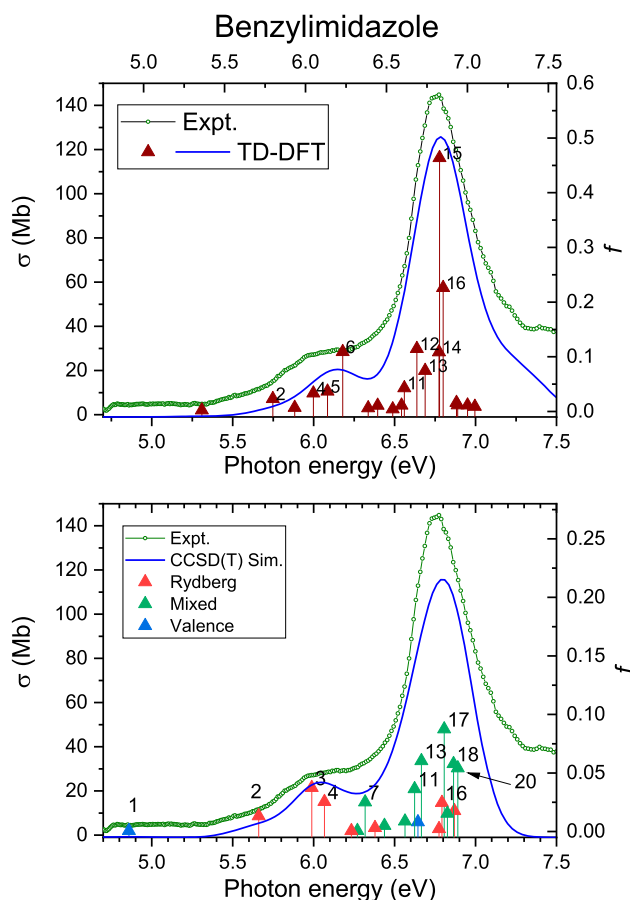
Figure 8. Theoretically predicted electronically excited states of 1-benzylimidazole (Table 5) and the absolute photoabsorption cross-section, σ, measured in the present study. Excited state numbering, transition energies, oscillator strengths, f, and assignments are given in Table 5. Other details as for Figure 5.

upon the CCSD calculated energies by adding a perturbation correction term for triple substitutions in the excited states. As with the ph-imid results, this also suggests a reason for some apparent deficiencies in the TD-DFT results. The corrected CCSD(T) energies are included in Table 5 (and the simulation in Figure 8) and are used to frame the following discussion.

The NTO analysis to identify the character of the excited states is summarised in Table 5. In many cases these descriptions are less definitive than was the case for ph-imid. For several of the excited states no single NTO hole-particle pair represents $\geq 50\%$ of the transition amplitude, and often two or even three NTO pairs need to be considered. Secondly, because of the anisotropic potential of the molecular core, the diffuse electron plots may deviate from a simple hydrogenic form (s, p, etc.) making them hard to describe. This appears to be a more significant issue with bz-imid, possibly resulting from the destruction of the quasi planar ph-imid structure (with only a small twist angle between the two ring structures)

caused by the incorporation of an additional linking C atom in the bz-imid structure. In Table 5 the descriptors of those Rydberg states that appear most distorted, and so can only be described approximately, are qualified by appearing in quotation marks. These problems notwithstanding, the inferred classification of states as essentially pure valence, pure Rydberg, or mixed Rydberg–valence character is corroborated by variations in the spatial extents, $\Delta\langle R^2\rangle$, that appear superimposed on the expected trend of steady increase of Rydberg size with increased excitation.

Considering now the interpretation of the experimental spectrum in terms of our theoretical coupled cluster results (Table 5, Figure 8), it can be seen that the first excitation, state #1 has a calculated CCSD(T) excitation energy of 4.75 eV. From the NTO analysis it is clearly analogous to the $1e_{1g}\ \pi \rightarrow 1e_{2u}\ \pi^*\ B_{2u}$ transition in benzene (and to the first excitation in ph-imid). In benzene this transition has a calculated energy of 4.70 eV and experimentally sits at 4.9 eV. While in the D_{6h} symmetry of benzene this $\pi \rightarrow \pi^*$ transition is one-photon forbidden (it only acquires a low experimental intensity through vibronic interaction), in bz-imid it is predicted to have a weak dipole oscillator strength. From the simulated and experimental bz-imid spectra in Figure 8 it can be seen that this weak excitation #1 must contribute the long but shallow onset in the 5 eV region of the bz-imid spectrum.

The next three states in bz-imid (#2–#4) involve excitation from the bz-imid HOMO, which is similar to the 3a" HOMO in imidazole (Table 1). The excited states are, respectively, 3s, and two 3p Rydberg states, that are predominantly centred at the imidazole ring, from where the transitions originate. As an example, the excited NTO for #2 is shown in Figure 9. Thus, states #2–#4 in bz-imid are loosely analogous to states #1–#3 in imidazole (Table 3). Transitions to these three states in bz-imid can convincingly account for the first, smaller peak seen in the experimental spectrum ~ 6 eV (Figure 8).

The next significant excitation in the simulation is to state #7, which contributes intensity between the first and second peaks of the spectrum. This transition is not well described by a single NTO hole–electron pair, but from the two leading pairs can be described as excitation from an initial orbital with $p\pi$ density over both rings to a mixed orbital/state displaying localised benzene $p\pi$ (e_{2u} symmetry) valence character plus a distorted p-type diffuse component (see Figure 10).

Overall, states #11, #13, #17, #18 and #20, all of which possess a significant oscillator strength and are predicted to occur in the energy range ~ 6.51–6.81 eV, would
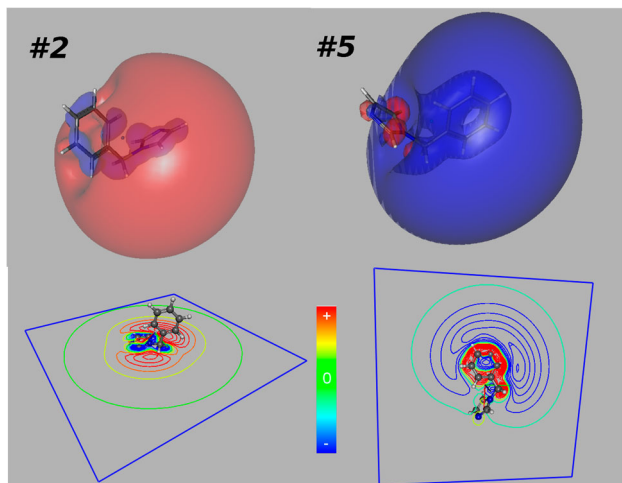
Figure 9. The NTO plots for the 3s Rydberg excited states #2 and #5 in 1-benzylimidazole. In the top row the 3-dimensional views are rendered with a translucent isosurface, and this permits some of the internal radial nodal structure to be seen. Note the 3s orbital is centred around the imidazole ring in #2, but the phenyl ring #5. In the bottom row are contour plots for #2 and #5 drawn in the plane of the imidazole and phenyl rings respectively, giving a clearer view of the radial nodes appearing at the interior and exterior of the respective ring. In both cases the plot region extends ± 22 a_0 along each axis.
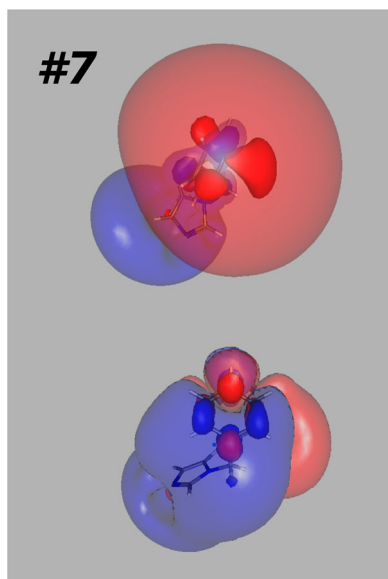

Figure 10. Iso-surface plots for excited state #7 of 1-benzylimidazole. The NTO analysis for the transition to #7 returns two leading hole–electron pairs, and both the excited NTO orbitals are shown here. The inner surfaces (value 0.045) are opaque and reveal the pπ valence structure on the phenyl ring; the outer surfaces (value 0.005) are rendered transparent to make the molecular frame and valence features visible.

appear to form the dominant contributions to the broad peak observed around 6.75 eV in the experimental spectrum.
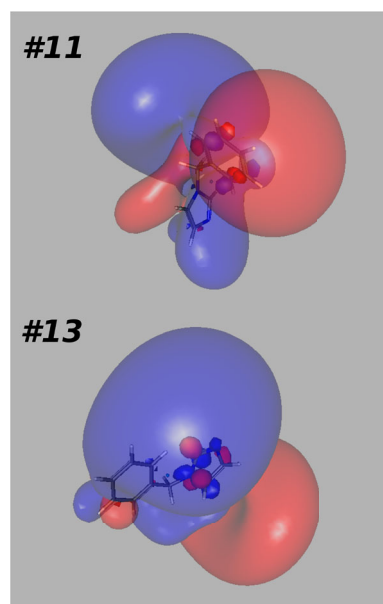

Figure 11. NTO plots for excited states #11 and #13 of benzylimidazole. The inner, opaque iso-surfaces (value 0.045) reveal localised valence character around, respectively, the phenyl and imidazole rings, while the transparent outer iso-surfaces (value 0.005) rather approximately resemble p type Rydberg orbitals.

States #11 and #13 both involve the excitation of mixed Rydberg/valence character (see Figure 11). The transition to state #11 is from an initial NTO pπ orbital extending over the whole molecule (resembling a combination of benzene and imidazole HOMO-like structure) to a more localised valence pπ structure on the phenyl ring (approximating e_{2u} symmetry) plus a diffuse Rydberg state of non-hydrogenic appearance. The state #13 transition is from the bz-imid HOMO (imidazole pπ orbital) to a mixed state with pπ valence density that remains localised on the imidazole ring plus a diffuse p-type Rydberg character.

The formation of states #17 to #20 can all be considered as d Rydberg excitations mixed with differing pπ valence excitation localised on the phenyl ring (see Figure 12). However, the valence excitation is weaker in #18 where it is evident only in the second NTO transition term. It may be noted that state #19 is a pure d Rydberg excitation, as also evident in its larger $\langle R^2 \rangle$ value (Table 5), and this would explain the much-reduced oscillator strength for its transition compared to the other excitations having d-Rydberg character.

In the foregoing discussion we have noted that the valence component of the mixed states #7 and #11 displays a partial shift of the initial delocalised π electron density towards the phenyl ring. While the transition #10 has too low an oscillator strength to significantly contribute to the spectrum, it more clearly demonstrates the
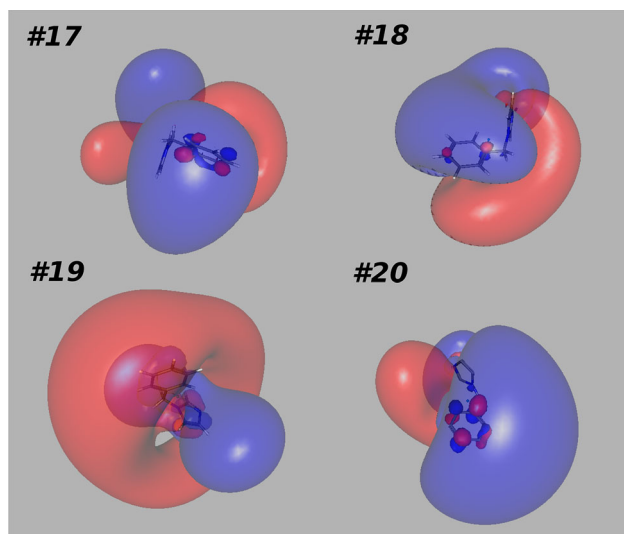
Figure 12. Benzylimidazole excited states: (top) the principle NTO transition term for #17 and the second NTO transition term for #18 showing only weak valence character for this latter excitation. (bottom) State #19, essentially a pure Rydberg d excitation, and state #20, another mixed Rydberg/pπ valence excitation. The inner (valence) iso-surfaces (value 0.03–0.04) are opaque, the outer diffuse surfaces (value 0.005) are rendered transparent.
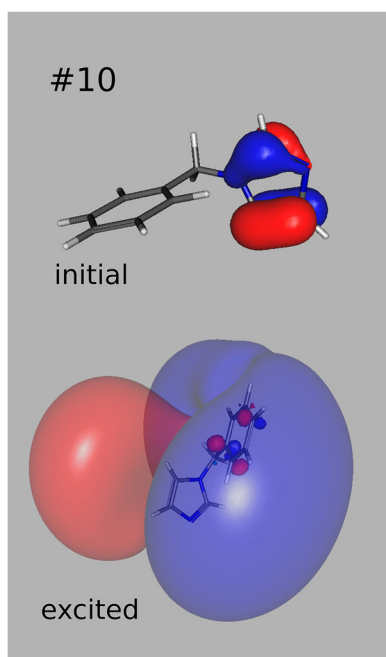

Figure 13. Iso-surface plots of the hole–electron NTO pair for the benzylimidazole transition to state #10. The valence iso-surfaces (value 0.04) are opaque, the outer diffuse surface for the mixed Rydberg/valence excited NTO (value 0.005) is transparently rendered. The valence π density transfers from the imidazole ring to the phenyl ring in this excitation.

valence charge transfer on excitation (see Figure 13). Its initial NTO is the bz-imid HOMO, a π orbital on the imidazole ring, while the mixed Rydberg valence excited

state #10 has a valence π component that has been transferred onto the phenyl ring. Hence, its transition can be viewed, like those for states #6—#8 in ph-imid (Figure 6), as a π–π charge transfer processes from an imidazole ring donor to a phenyl ring acceptor.

5. Summary

This paper reports a combined theoretical and experimental investigation of the VUV absorption spectroscopy of two substituted imidazole molecules, 1-phenylimidazole and 1-benzylimidazole, with a focus on attributing valence, Rydberg, or mixed Rydberg–valence character to their electronically excited states. In both molecules a preliminary examination of the outermost occupied valence orbitals has revealed some strong similarities with the outermost orbitals of their isolated constituent ring systems. Anticipating the possibility that some electronic excitations may also resemble transitions localised in one or other of the constituent rings we have commenced the report by revisiting the electronic spectroscopy of benzene and imidazole. In the case of benzene, EOM-CCSD(T) calculations have been used to improve estimates of the 3p and 3d Rydberg excitation energies, thereby providing clarity on the two broad absorption bands recorded between 6.0 and 7.5 eV in the VUV absorption spectrum. For imidazole, our earlier reported TD-DFT electronic state calculations [1] have been updated and extended with new EOM-CCSD(T) results.

The experimental spectra of ph-imid and bz-imid lacked the well-resolved structure seen in the imidazole VUV absorption. Simulations of the absorption band profiles were thus generated by folding a relatively broad Gaussian shaping function into the calculated stick spectra. The TD-DFT and EOM-CCSD simulation results both provided rather convincing reproduction of the experimental bands, but a more detailed state-by-state comparison of these two methods revealed deficiencies such as missed states in the TD-DFT case. Given well-known difficulties of this method when two-electron and charge transfer excitations may be involved, and its increasing unreliability when pushed to higher excitations, the higher-level EOM-CCSD results were preferred as a basis for subsequent discussion.

The first excitation in both ph-imid and bz-imid shows a clear resemblance to the first $1e_{1g} \rightarrow 1e_{2u}$ B_{2u} transition in benzene. Although no longer dipole forbidden in the lowered symmetry of these substituted systems, they remain very weak in the experimental spectra. Experimentally, the two molecular spectra look very similar, yet the calculations predict that the dominant transitions under the first, weaker band (5.3 eV in ph-imid, $\sim$6 eV

in bz-imid) are valence $\pi \rightarrow \pi^*$ excitations (#2, #4) in ph-imid, but low-lying 3s, 3p Rydberg excitations (#2, #3, #4) in bz-imid.

The larger of the two peaks in the ph-imid spectrum (~ 6.7 eV) results from a variety of Rydberg and mixed Rydberg/valence transitions, but with the most intense representing transitions with a diffuse 3d Rydberg character. The corresponding experimental peak in bz-imid (~ 6.75 eV) also spans several predicted Rydberg and mixed Rydberg/valence excitations. Here the diffuse character is not so readily describable by simple hydrogenic orbital patterns but is of predominantly p/d type.

Lying between the two experimental peaks in both molecules are predicted transitions with much less oscillator strength, but nevertheless that are worth noting. In ph-imid, these are the mixed valence π/3p excitations starting from ~ 5.9 eV (#6–#8) and these are particularly interesting as the transitions are from the HOMO, an imidazole ring localised π orbital, to phenyl ring localised π orbitals mixed with a diffuse 3p contribution (Figure 6). Thus, it appears that there is an effective intramolecular charge transfer from an imidazole ring donor to the phenyl ring acceptor. Similar imidazole $\rightarrow$ phenyl charge transfer characteristics were noted in the ph-imid #18 and the bz-imid #10 mixed Rydberg/valence excitations (Figures 7 and 13 respectively) with an element of imidazole $\rightarrow$ phenyl charge transfer also having been commented upon in the bz-imid states #7 and #11. These states evidence a unique donor–acceptor preference by that part of the excited Rydberg electron density that is 'recaptured' within the nascent molecular ion core of the Rydberg state, associating with the phenyl- rather than the imidazole-ring. This may be part rationalised on energetic grounds by noting that benzene has a greater binding (ionisation) energy than imidazole (see Table S2, Supplementary Material).

Disclosure statement

No potential conflict of interest was reported by the author(s).

Funding

References

[1] D.M.P. Holland, D.A. Shaw, D. Townsend and I. Powis, Mol. Phys. **121** (7-8), e2122614 (2023). doi:10.1080/00268976.2022.2122614.

[2] R.L. Martin, J. Chem. Phys. **118** (11), 4775 (2003). doi:10.1063/1.1558471; F. Plasser, M. Wormit and A. Dreuw, J. Chem. Phys. **141** (2), 024106 (2014); F. Plasser, S.A. Bappler, M. Wormit and A. Dreuw, J. Chem. Phys. **141** (2), 024107 (2014).

[3] V. May and O. Kuhn, *Charge and Energy Transfer Dynamics in Molecular Systems* (Wiley-VCH, Weinheim, 2011); H.J. Wörner, C.A. Arrell, N. Banerji, A. Cannizzo, M. Chergui, A.K. Das, P. Hamm, U. Keller, P.M. Kraus, E. Liberatore, P. Lopez-Tarifa, M. Lucchini, M. Meuwly, C. Milne, J.E. Moser, U. Rothlisberger, G. Smolentsev, J. Teuscher, J.A. van Bokhoven and O. Wenger, Struct. Dyn.-US **4** (6), 38, 061508 (2017).

[4] P.G. Wilkinson, Can. J. Phys. **34** (6), 596 (1956). doi:10.1139/p56-067.

[5] E.E. Koch and A. Otto, Chem. Phys. Lett. **12** (3), 476 (1972). doi:10.1016/0009-2614(72)90011-5; D. G. Wilden and J. Comer, J. Phys. B-At. Mol. Opt. Phys. **13** (3), 627 (1980); E.E. Rennie, C.A.F. Johnson, J. E. Parker, D.M.P. Holland, D.A. Shaw and M.A. Hayes, Chem. Phys. **229** (1), 107 (1998); F.J. Capalbo, Y. Bénilan, N. Fray, M. Schwell, N. Champion, E.T. Es-Sebbar, T.T. Koskinen, I. Lehocki and R. V. Yelle, Icarus **265**, 95 (2016).

[6] A. Hiraya and K. Shobatake, J. Chem. Phys. **94** (12), 7700 (1991). doi:10.1063/1.460155.

[7] A. Dawes, N. Pascual, S.V. Hoffmann, N.C. Jones and N.J. Mason, Phys. Chem. Chem. Phys. **19** (40), 27544 (2017). doi:10.1039/C7CP05319C.

[8] J. Lorentzon, P.A. Malmqvist, M. Fulscher and B.O. Roos, Theor. Chim. Acta. **91** (1-2), 91 (1995). doi:10.1007/BF01113865; N.C. Handy and D.J. Tozer, J. Comput. Chem. **20** (1), 106 (1999).

[9] M.J. Packer, E.K. Dalskov, T. Enevoldsen, H.J.A. Jensen and J. Oddershede, J. Chem. Phys. **105** (14), 5886 (1996). doi:10.1063/1.472430; J.E. DelBene, J.D. Watts and R.J. Bartlett, J. Chem. Phys. **106** (14), 6051 (1997); M. Schreiber, M.R. Silva-Junior, S.P.A. Sauer and W. Thiel, J. Chem. Phys. **128** (13), 134110 (2008); H.H. Falden, K.R. Falster-Hansen, K.L. Bak, S. Rettrup and S.P.A. Sauer, J. Phys. Chem. A **113** (43), 11995 (2009); P.F. Loos, M. Boggio-Pasqua, A. Scemama, M. Caffarel and D. Jacquemin, J. Chem. Theory Comput. **15** (3), 1939 (2019); P.F. Loos, F. Lipparini, M. Boggio-Pasqua, A. Scemama and D. Jacquemin, J. Chem. Theory Comput. **16** (3), 1711 (2020); R. Sarkar, P.F. Loos, M. Boggio-Pasqua and D. Jacquemin, J. Chem. Theory Comput. **18** (4), 2418 (2022).

[10] O. Christiansen, H. Koch, A. Halkier, P. Jorgensen, T. Helgaker and A.S. de Meras, J. Chem. Phys. **105** (16), 6921 (1996). doi:10.1063/1.471985.

[11] A. Bernhardsson, N. Forsberg, P. Malmqvist, B.O. Roos and L. Serrano-Andrés, J. Chem. Phys. **112** (6), 2798 (2000). doi:10.1063/1.480854.

[12] T.J. Penfold and G.A. Worth, J. Chem. Phys. **131** (6), 064303 (2009). doi:10.1063/1.3197555.

[13] P.M. Johnson, J. Chem. Phys. **64** (10), 4143 (1976). doi:10.1063/1.431983; R.L. Whetten, S.G. Grubb, C.E. Otis, A.C. Albrecht and E.R. Grant, J. Chem. Phys. **82** (3), 1115 (1985); S.G. Grubb, C.E. Otis, R.L. Whetten, E.R. Grant and A.C. Albrecht, J. Chem. Phys. **82** (3), 1135 (1985).

[14] P.M. Johnson and G.M. Korenowski, Chem. Phys. Lett. **97** (1), 53 (1983). doi:10.1016/0009-2614(83)87182-6; R.L.

Whetten, K.J. Fu and E.R. Grant, J. Chem. Phys. **79** (6), 2626 (1983).

[15] M. Patanen, A.R. Abid, S.T. Pratt, A. Kivimäki, A.B. Trofimov, A.D. Skitnevskaya, E.K. Grigoricheva, E.V. Gromov, I. Powis and D.M.P. Holland, J. Chem. Phys. **155**, 054304 (2021). doi:10.1063/5.0058983.

[16] M.J. Paterson and D. Townsend, Int. Rev. Phys. Chem. **39** (4), 517 (2020). doi:10.1080/0144235X.2020.1815389.

[17] D.M.P. Holland, D.A. Shaw, I.C. Walker, I.J. McEwen and M.F. Guest, Chem. Phys. **344** (3), 227 (2008). doi:10.1016/j.chemphys.2008.01.006.

[18] D.M.P. Holland, J.B. West, A.A. Macdowell, I.H. Munro and A.G. Beckett, Nucl. Instrum. Methods Phys. Res. B. **44** (2), 233 (1989). doi:10.1016/0168-583X(89)90433-3.

[19] D. M. P. Holland, Phys. Scrip. **36** (1), 22 (1987). doi:10.1088/0031-8949/36/1/004.

[20] D.A. Shaw, D.M.P. Holland, M.A. Macdonald, A. Hopkirk, M.A. Hayes and S.M. McSweeney, Chem. Phys. **163** (3), 387 (1992). doi:10.1016/0301-0104(92)87119-T.

[21] D.M.P. Holland, D.A. Shaw, S. Coriani, M. Stener and P. Decleva, J. Phys. B-At. Mol. Opt. Phys. **46** (17), 175103 (2013). doi:10.1088/0953-4075/46/17/175103.

[22] G. Herzberg, *Molecular Spectra and Molecular Structure III. Electronic Spectra and Electronic Structure of Polyatomic Molecules* (D. Van Nostrand, New York, 1966).

[23] J.F. Stanton and R.J. Bartlett, J. Chem. Phys. **98** (9), 7029 (1993). doi:10.1063/1.464746.

[24] E. Epifanovsky, A.T.B. Gilbert, X. Feng, J. Lee, Y. Mao, N. Mardirossian, P. Pokhilko, A.F. White, M.P. Coons, A.L. Dempwolff, Z. Gan, D. Hait, P.R. Horn, L.D. Jacobson, I. Kaliman, J. Kussmann, A.W. Lange, K.U. Lao, D.S. Levine, J. Liu, S.C. McKenzie, A.F. Morrison, K.D. Nanda, F. Plasser, D.R. Rehn, M.L. Vidal, Z.-Q. You, Y. Zhu, B. Alam, B.J. Albrecht, A. Aldossary, E. Alguire, J.H. Andersen, V. Athavale, D. Barton, K. Begam, A. Behn, N. Bellonzi, Y.A. Bernard, E.J. Berquist, H.G.A. Burton, A. Carreras, K. Carter-Fenk, R. Chakraborty, A.D. Chien, K.D. Closser, V. Cofer-Shabica, S. Dasgupta, M.d. Wergifosse, J. Deng, M. Diedenhofen, H. Do, S. Ehlert, P.-T. Fang, S. Fatehi, Q. Feng, T. Friedhoff, J. Gayvert, Q. Ge, G. Gidofalvi, M. Goldey, J. Gomes, C.E. González-Espinoza, S. Gulania, A.O. Gunina, M.W.D. Hanson-Heine, P.H.P. Harbach, A. Hauser, M.F. Herbst, M.H. Vera, M. Hodecker, Z.C. Holden, S. Houck, X. Huang, K. Hui, B.C. Huynh, M. Ivanov, Á Jász, H. Ji, H. Jiang, B. Kaduk, S. Kähler, K. Khistyaev, J. Kim, G. Kis, P. Klunzinger, Z. Koczor-Benda, J.H. Koh, D. Kosenkov, L. Koulias, T. Kowalczyk, C.M. Krauter, K. Kue, A. Kunitsa, T. Kus, I. Ladjánszki, A. Landau, K.V. Lawler, D. Lefrancois, S. Lehtola, R.R. Li, Y.-P. Li, J. Liang, M. Liebenthal, H.-H. Lin, Y.-S. Lin, F. Liu, K.-Y. Liu, M. Loipersberger, A. Luenser, A. Manjanath, P. Manohar, E. Mansoor, S.F. Manzer, S.-P. Mao, A.V. Marenich, T. Markovich, S. Mason, S.A. Maurer, P.F. McLaughlin, M.F.S.J. Menger, J.-M. Mewes, S.A. Mewes, P. Morgante, J.W. Mullinax, K.J. Oosterbaan, G. Paran, A.C. Paul, S.K. Paul, F. Pavošević, Z. Pei, S. Prager, E.I. Proynov, Á. Rák, E. Ramos-Cordoba, B. Rana, A.E. Rask, A. Rettig, R.M. Richard, F. Rob, E. Rossomme, T. Scheele, M. Scheurer, M. Schneider, N. Sergueev, S.M. Sharada, W. Skomorowski, D.W. Small, C.J. Stein, Y.-C. Su, E.J. Sundstrom, Z. Tao, J. Thirman, G.J. Tornai, T. Tsuchimochi, N.M. Tubman, S.P. Veccham, O. Vydrov, J. Wenzel, J. Witte, A. Yamada, K. Yao, S. Yeganeh, S.R. Yost, A. Zech, I.Y. Zhang, X. Zhang, Y. Zhang, D. Zuev, A. Aspuru-Guzik, A.T. Bell, N.A. Besley, K.B. Bravaya, B.R. Brooks, D. Casanova, J.-D. Chai, S. Coriani, C.J. Cramer, G. Cserey, A.E. DePrinceIII, R.A. DiStasioJr., A. Dreuw, B.D. Dunietz, T.R. Furlani, W.A. Goddard-III, S. Hammes-Schiffer, T. Head-Gordon, W.J. Hehre, C.-P. Hsu, T.-C. Jagau, Y. Jung, A. Klamt, J. Kong, D.S. Lambrecht, W. Liang, N.J. Mayhall, C.W. McCurdy, J.B. Neaton, C. Ochsenfeld, J.A. Parkhill, R. Peverati, V.A. Rassolov, Y. Shao, L.V. Slipchenko, T. Stauch, R.P. Steele, J.E. Subotnik, A.J.W. Thom, A. Tkatchenko, D.G. Truhlar, T.V. Voorhis, T.A. Wesolowski, K.B. Whaley, H.L. WoodcockIII, P.M. Zimmerman, S. Faraji, P.M.W. Gill, M. Head-Gordon, J.M. Herbert and A.I. Krylov, J. Chem. Phys. **155** (8), 084801 (2021). doi:10.1063/5.0055522.

[25] K. Kaufmann, W. Baumeister and M. Jungen, J. Phys. B-At. Mol. Opt. Phys. **22** (14), 2223 (1989). doi:10.1088/0953-4075/22/14/007.

[26] D.P. Singh, N. de Oliveira, G. Garcia, A. Vredenborg and I. Powis, ChemPhysChem. **21**, 2468 (2020). doi:10.1002/cphc.202000365.

[27] H. Ganjitabar, D.P. Singh, R. Chapman, A. Gardner, R.S. Minns, I. Powis, K.L. Reid and A. Vredenborg, Mol. Phys. **119** (1-2), e1808907 (2020). doi:10.1080/00268976.2020.1808907.

[28] P. Baltzer, L. Karlsson, B. Wannberg, G. Ohrwall, D.M.P. Holland, M.A. MacDonald, M.A. Hayes and W. von Niessen, Chem. Phys. **224** (1), 95 (1997). doi:10.1016/S0301-0104(97)00244-9.

[29] M. Robin, *Higher Excited States of Polyatomic Molecules* (Academic Press, Orlando, 1985).

[30] H. Keller-Rudek, G.K. Moortgat, R. Sander and R. Sörensen, Earth Syst. Sci. Data. **5** (2), 365 (2013).

[31] R.L. Whetten and E.R. Grant, J. Chem. Phys. **80** (12), 5999 (1984). doi:10.1063/1.446681; A. Staib and W. Domcke, J. Chem. Phys. **94** (8), 5402 (1991).

[32] M.J.G. Peach, T. Helgaker, P. Salek, T.W. Keal, O.B. Lutnaes, D.J. Tozer and N.C. Handy. Phys. Chem. Chem. Phys. **8** (5), 558 (2006). doi:10.1039/B511865D.